
National Laboratory for Scientific Computing
Av. Getúlio Vargas 333
Petrópolis, Rio de Janeiro
Brazil

1st LNCC Meeting on
Computational Modelling
August 9–13, 2004

Multidimensional Models of Stenotic Carotid Bifurcations

Santiago A. Urquiza, Pablo J. Blanco

Laboratorio de Bioingeniería, Universidad Nacional de Mar del Plata
Av. J.B. Justo 4302, 7600 Mar del Plata, Argentina
Email: santiagourquiza@fi.mdp.edu.ar

Marcelo J. Vénere

PLADEMA–CNEA, Facultad de Exactas, Universidad Nacional del Centro de la Provincia de Buenos Aires
Pinto 399, 7000 Tandil, Argentina
Email: venerem@exa.unicen.edu.ar

Raúl A. Feijóo

LNCC, Laboratório Nacional de Computação Científica
Av. Getulio Vargas 333, Quitandinha, 25651-075, Petrópolis, RJ, Brasil
Email: feij@lncc.br

Abstract. A multi-dimensional hemodynamic model is used to analyze the flow patterns due to the presence of stenosis in a carotid artery. A three-dimensional model corresponding to the carotid bifurcation is embedded in a one-dimensional representation for the rest of the human arterial tree. In this way, it is possible to provide with proper boundary conditions the derived Navier-Stokes problem in compliant domains related to the 3D carotid model. The 1D representation of the whole arterial system is obtained by reducing the equations of mass and moment conservation in compliant vessels. Additionally, the peripheral beds are implemented through the well-known Windkessel model. The 3D meshes associated with the carotid bifurcation are derived from a standard geometry in which two stenosis levels are introduced strangling the carotid sinus. Detailed flow patterns in the carotid bifurcation are provided. More realistic flow and pressure curves are obtained when wall viscosity is introduced. Also, it is shown that the pulse shape is considerably influenced by the heart inflow condition. These techniques may be a valuable aid as they supply complementary elements of analysis that can facilitate the understanding of the hemodynamic conditions that promote the onset and progress of this kind of vessel affections.

Key Words: Haemodynamics, FEM, Fluid-structure Interaction, Coupling 3D-1D, Stenosis.

1 Introduction

As vascular diseases have become one of the main death causes in the occidental world, an increasingly number of research efforts has been tackling the associated problems with the aim of improving therapeutic, prevention and diagnostic techniques. Among others, atherosclerosis is one of the most prevalent pathology. Clinical investigations reveal that atheroma plaques are mainly localized in vascular districts where altered hemodynamic conditions are present[1],[2]-[5],[32]. These zones are characterized by irregularities in the blood flow structure, such as flow separation and reversal, as well as low oscillatory wall shear stresses.

The Computational Modelling plays a decisive role in the progress of this research field. This is mainly due to *in vivo* experiments are limited by lots of practical and ethical obstacles. Nowadays, is possible to implement complex realistic computational models so as to acquire a better understanding of the hemodynamic phenomena present in the human arterial system, at very low cost and without inconveniencing people. In this way, computational models arise as powerful tools to improve diagnostics and surgery strategies.

Arterial system modelling implies some challenging issues as geometry reconstruction from medical images (MRI, CAT, etc.)[2],[6]-[8],[23] and numerical solution of non-linear problems which involve the fluid-structure interaction between the blood flow and the compliant arterial walls. As 3D models of the whole arterial system remain prohibitive from a computational point of view, it is only viable to model -with a high degree of detail- small portions of the arterial tree. Furthermore, it is only possible to use local representations so as to study the phenomena associated to the flow dynamics in districts such as bifurcations and other singularities. In this way, rather detailed descriptions of vortex development and wall shear stresses-among other relevant hemodynamic phenomena- may be obtained in those locations. But, the implementation of these local models introduces artificial boundaries where proper conditions must be supplied. There, spurious reflexions must be avoided[36]-[40] and also, it is necessary to specified contour conditions that take into account the interactions with the rest of the arterial system in a time dependant context. This is due to the arterial pulse propagates along the whole arterial tree. As a result, local perturbations can travel long distances affecting far away districts either upstream or downstream. In order to avoid such difficulties, appropriate coupling between complex 3D models and reduced 1D models must be considered. These 1D models are used to represent the rest of the arterial system supplying the formers with proper boundary conditions that take into account the systemic interactions. With this approach, boundary conditions for localized models will be naturally adjusted when changes occurs in any of the two models. This in turn, facilitates the implementation of different situations of practical interest with easy.

In this work we present an analysis of the hemodynamic behavior of carotid bifurcations where different stenosis strengths are introduced. These districts are represented multidimensionally, based on a standard geometry to facilitate testing and comparisons with other researchers. The rest of the arterial tree is modeled with a reduced 1D model. Additionally, it is also addressed how the parietal viscosity and the inflow boundary condition representing the cardiac ejection influence the pulse wave shape.

2 Governing equations

2.1 The one-dimensional model

Blood flow through the arteries can be considered as the flow of an incompressible fluid in straight compliant vessels. Therefore, it is possible to obtain the governing equations from the mass and momentum conservation equations, integrating the relevant quantities on the transversal area. The result is the following non-linear system of partial differential equations[13]:

$$\frac{\partial Q}{\partial t} + \frac{\partial}{\partial x}\left(\alpha \frac{Q^2}{A}\right) = -\frac{A}{\rho} \frac{\partial P}{\partial x} - \frac{p.D}{\rho}\, .t_o \tag{1}$$

$$\frac{\partial A}{\partial t} + \frac{\partial Q}{\partial x} = 0 \tag{2}$$

with

$$\alpha = \frac{A\int u^2 dA}{Q^2} \quad ; \quad t_o = f_r . \frac{\rho . \tilde{u} . |\tilde{u}|}{8} \quad ; \quad Q = \tilde{u} . A \; ; \tag{3}$$

where A is the artery section, u is the axial velocity ($\tilde{u}$ is the corresponding mean value), x is the axial coordinate, P is the mean pressure, ρ is the blood density, t_o is the wall shear stress due to viscosity acting against the wall being f_r the Darcy friction factor (here a fully developed parabolic profile was considered) and α is a correction factor for the axial momentum, $\alpha = 1$ is used along this work.
An equation representing the arterial wall behavior is also needed. A linear viscoelastic constitutive relationship is considered. Taking into account the equilibrium equation for a thin walled tube, the following equation was adopted,

$$P = P_o + \frac{E\rho R_o h_o}{A}\left[\sqrt{\frac{A}{A_o}} - 1\right] + \frac{k\rho R_o h_o}{A} \frac{1}{2\sqrt{A_o A}} \frac{\partial A}{\partial t} \tag{4}$$

where R_o, h_o and A_o are radius, wall thickness and area referred to the outer pressure value P_o, E is the effective Young modulus and k is the fluidity coefficient due to parietal viscosity.

2.2 The multidimensional model. Coupling equations

The behavior of the fluid within three-dimensional regions was described using the Navier-Stokes equations for incompressible Newtonian flows. Due to the arterial compliance, the domain moves according to the displacement of the walls. This was considered stating the problem in the context of an arbitrarily Lagrangian-Eulerian formulation[33] (ALE). The

following equations are applicable:

$$\begin{aligned} & r\frac{\partial \mathbf{u}}{\partial t} + r\,(\mathbf{u}-\mathbf{v})\cdot\tilde{\mathrm{N}}\,\mathbf{u} - m\tilde{\mathrm{N}}^2\mathbf{u} + \tilde{\mathrm{N}}\,P = \mathbf{f} \qquad \text{en } \Omega \\ & div\ \mathbf{u} = 0 \end{aligned} \tag{5}$$

$$\tilde{\mathrm{N}}^2\Delta\mathbf{x} = 0 \qquad \text{en } \Omega \tag{6}$$

where **u** is the fluid viscosity, **v** is the velocity of the reference frame consistent with the ALE formulation, *P* is the pressure field, $\Delta\mathbf{x}$ is the displacements vector for the deformable domain with respect to its reference configuration, **f** are the volume body forces and, ρ and μ are density and flow viscosity respectively. This set of equations must be provided with proper boundary conditions and a proper constitutive relation which links the displacement of the arterial wall with pressure. We have chosen the simple independent rings wall model[4],[37] consistent to that used for the 1D model. In this manner, the following equations were used for the surface points in $\partial\,\Omega_w$ -the surface representing the arterial wall-:

$$\begin{aligned} & P - P_o = \frac{E\,h}{R_o^2}\,d + \frac{k\,h}{R_o^2}\,\frac{dd}{dt} \\ & \Delta\mathbf{x} = d\,\mathbf{n} \qquad \text{en } \partial\,\Omega_w \\ & \mathbf{v} = \frac{d\,\Delta\mathbf{x}}{d\,t} \end{aligned} \tag{7}$$

where δ is the displacement of the nodes placed on the arterial wall normal to the surface (**n** is the normal vector to the surface). It is evident the analogy between the first of the equations (7) to that given in (4) for the 1D model.

In order to accomplish the coupling between the 1D model and the 3D model another set of equations must be specified on the interfaces to be connected, which states for the proper coupling conditions regarding a well-posed problem[28],[36]-[40]. Therefore, it is necessary to impose equations satisfying the continuity of mass, momentum and stresses on those interfaces. For the Reynolds number prevailing in the arterial system, the continuity upon the stresses reduces to pressure continuity[29],[37]. It is important to note that the continuity of the linear moment is implied in the election of the parameter α present in eq. (1), which should be obtained in a non-linear way from the 3D velocity profile. In the present work $\alpha = 1$ was used implying that the continuity on momentum is not fulfilled. However, the consideration of such situation does not produce significant spurious reflections in the cases of long wavelengths, which is the situation for the arterial tree. Thus, the proper coupling conditions between the two models are as follows:

$$
\begin{aligned}
& Q_i = -\int_{\partial\Omega_i} \mathbf{u}.\mathbf{n}\, dS \\
& \left\langle r\frac{\partial \mathbf{u}}{\partial t}, \mathbf{w} \right\rangle + \left\langle r(\mathbf{u}-\mathbf{v})\nabla\mathbf{u}, \mathbf{w} \right\rangle - \left\langle P, div\,\mathbf{w} \right\rangle + \left\langle m\nabla\mathbf{u}, \nabla\mathbf{w} \right\rangle = \\
& = \left\langle \mathbf{f}, \mathbf{w} \right\rangle + \sum_i \int_{\partial\Omega_i} -P_i \mathbf{n}.\mathbf{w}\, dS \quad \forall \mathbf{w} \in \mathbf{H}^1, i = 1,2,3
\end{aligned}
\tag{8}
$$

where P_i is the mean value of the pressure given by the 1D model in the coupling interfaces $\partial\,\Omega_i$, while Q_i is the corresponding 1D flow rate. The first of the equations (8) implies mass continuity, while the second is the variational counterpart of the first of the eq. (5), which implies the weak continuity on pressure, as the surface tractions were replaced by pressure P_i given by the 1D model. As was already mentioned, normal tractions coincide with the pressure for high Reynolds numbers.

3 Numerical approach

3.1 The physiological 1D model

The complete arterial system was modeled from the composition of 128 segments as shown in Fig. 1. This topology is based entirely in that proposed by Avolio[11]. There, geometrical and mechanical parameter values can also be found. Regarding the parietal viscosity, it is defined the angle f as $f = arctg\left(wk/E\right)$ where $w = 2p/T$, being T the heart period. This parameter is a measure of the relative magnitude of the parietal viscosity force to the elastic one.

For the inflow boundary condition, the flow ejected by the left ventricle at the aortic root was considered. In Fig. 2 the two curves used in this work are shown. These were taken from Spencer[18] and Stettler[21], as indicated. The original curves were normalized to a mean volume rate corresponding to 5 lt/min. On branches continuity on pressure and flow is considered [14].

In order to include the action of the peripheral beds, lumped Windkessel models[12],[14]-[16] are used. These elements comprise a resistance R_1 in series with the parallel of a resistance R_2 and a capacitor C. The values of the resistances are such that the flow distribution towards the different parts of the body is according to that given in [26], always verifying the relation $R_1 = 0.2\,R_T$ [12],[15] with $R_T = (R_1 + R_2)$. The total peripheral compliance is taken from Stergiopulos[12]. This compliance is distributed on each Windkessel terminal following the same guidelines proposed there. The equation which corresponds to each terminal is as follows:

$$
\frac{dQ}{dt} = \frac{1}{R_1 R_2 C}\left[R_2 C \frac{dP}{dt} + P - (R_1 + R_2)Q \right] \tag{9}
$$

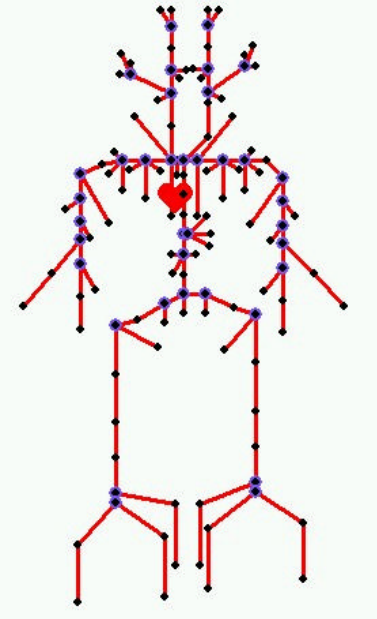

Fig. 1. Topology of the modeled arterial system.

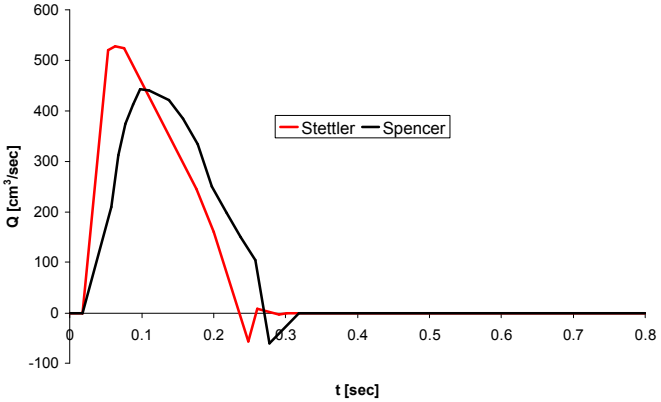

Fig. 2. Entrance flow conditions.

The one-dimensional model has 1212 nodes and 1326 linear elements. Equations (1), (2) and (4) are discretized by means of the Finite Element Method, using a Galerkin-Least Squares formulation over the characteristics lines corresponding to the normal equations associated with the resulting hyperbolic system when $k=0$. Such scheme is operated with a stabilization parameter corresponding to the optimal value for the SUPG[34] method. The implementation is made within the context of a framework[27] for the solution of discrete problems, which allows a simple and direct use of different kinds of elements despite their formulations or dimensions.

3.2 The 3D model

In order to solve the equations systems resulting for the 3D domains, again the Finite Element Method is used. A mesh o using a P1b-P1 interpolation of tetrahedral elements with bubble shape functions for the velocity field and linear for the scalar pressure field[35]. The equations are solved with the Finite Element SUPG Method[34], with a θ-Euler implicit finite difference scheme for the temporal derivates, using Picard iterations in order to treat the non-linear convective terms. The solution of the problem is split into three sub-steps: in the first one, the bubble degrees of freedom are eliminated by direct substitution and the N-S problem is solved using the pressure values obtained in 1D model in the previous time step as boundary conditions. In the second sub-step, we solve the bubble degrees of freedom to be used in the following time step, and finally, in the third one, the solution for the 1D model is obtained with the flow rate values obtained from the multidimensional model in the first sub-step. This process can be iterated up to the global convergence,

although the numerical experience shows that with a simple global iteration the results obtained do not noticeable vary in the subsequent steps. This coupling alternative does not require the calculation of the Riemann invariants in contrast with that proposed in [37]. The domain is updated from the position of the nodes on the surface -that are obtained from eq. (7)- solving a Laplace problem for each coordinate associated with the interior nodes' position.

The 3D geometry, shown in Fig. 3, upon which the present work is developed, was proposed by Bharadvaj et. al.[41],[42] and scaled in this work for being consistent with the common carotid diameter value of the 1D model. From this one, both stenoses were done according to that shown in Fig. 3. In such figure the dimensions are given along the axis corresponding to each segment. In Table 1 are specified the diameters in the considered sections which define the geometry used of the carotid bifurcation for the stenosis severities studied. The percentage of stenosis is specified as the percentage of area reduction on section SS3 relative to the normal case.

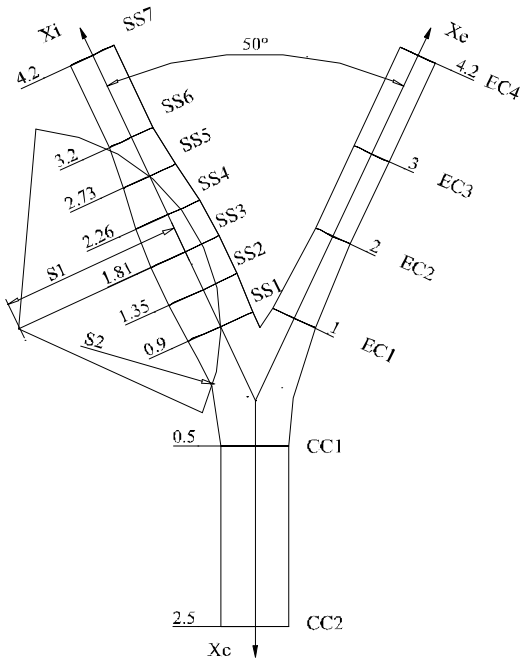

Fig. 3. Base geometry and stenosis morphology.

Section	Diameter [cm]	
CC1	0.74	
CC2	0.74	
SS1	0.77182	
SS2	0.8214	
SS3	0.8214	
SS4	0.76368	
SS5	0.6364	
SS6	0.5254	
SS7	0.5254	
EC1	0.51356	
EC2	0.42032	
EC3	0.42032	
EC4	0.42032	
References (stenosis)	**S [cm]**	
	80%	**95%**
S1	2	1.5
S2	2.20535	1.835

Table 1. Geometric parameters.

In Table 2 the total number of nodes, tetrahedral and triangular elements are specified for each of the three cases. The triangular elements are related to the arteial wall model and also with the coupling interfaces between the 1D and the 3D models. From now on, we should name *N*, *S80* y *S95* the cases for the normal carotid, and carotid with 80% and 95%

of stenosis, respectively.

Model	Tetrahedral	Triangles	Nodes
N	294075	28000	55794
S80	198154	26034	40373
S95	370562	30190	69156

Table 2. Mesh characteristics.

Details of the surface mesh are shown for each case in Fig. 4 to Fig. 6. Also, the corresponding volume meshes are illustrated in Fig. 7 to Fig. 9.

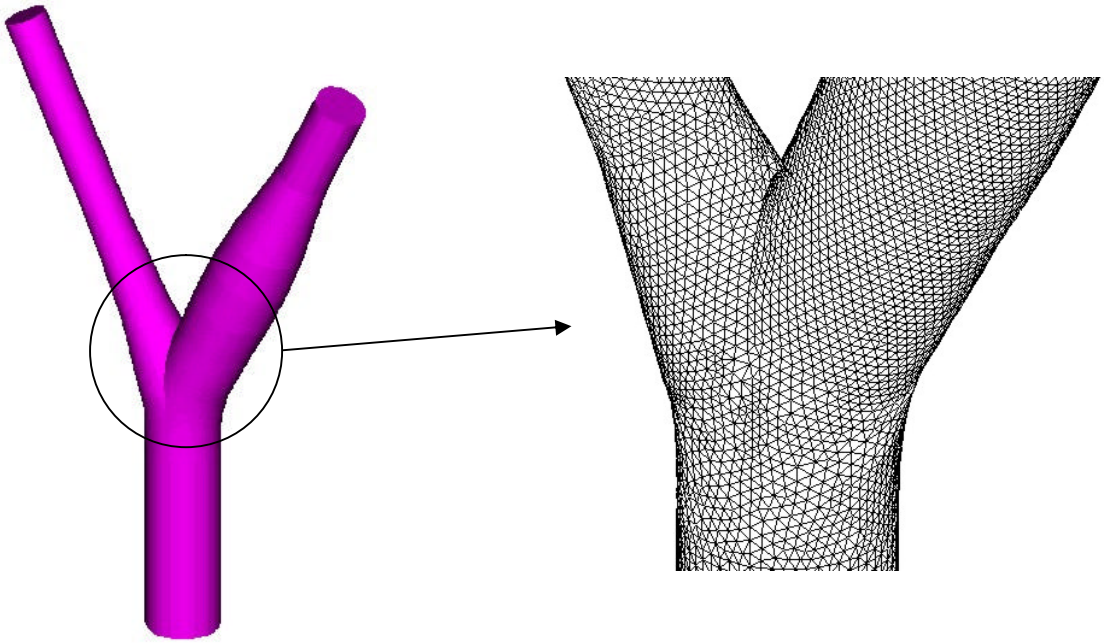

Fig. 4. Case *N*. Geometry and surface mesh.

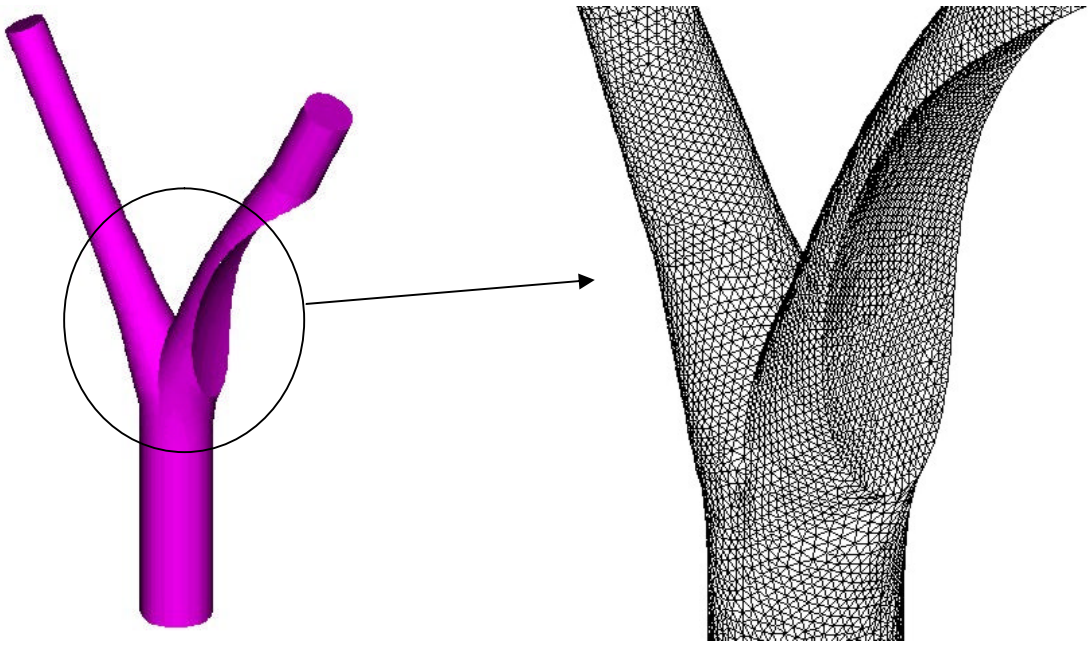

Fig. 5. Case *S80*. Geometry and surface mesh.

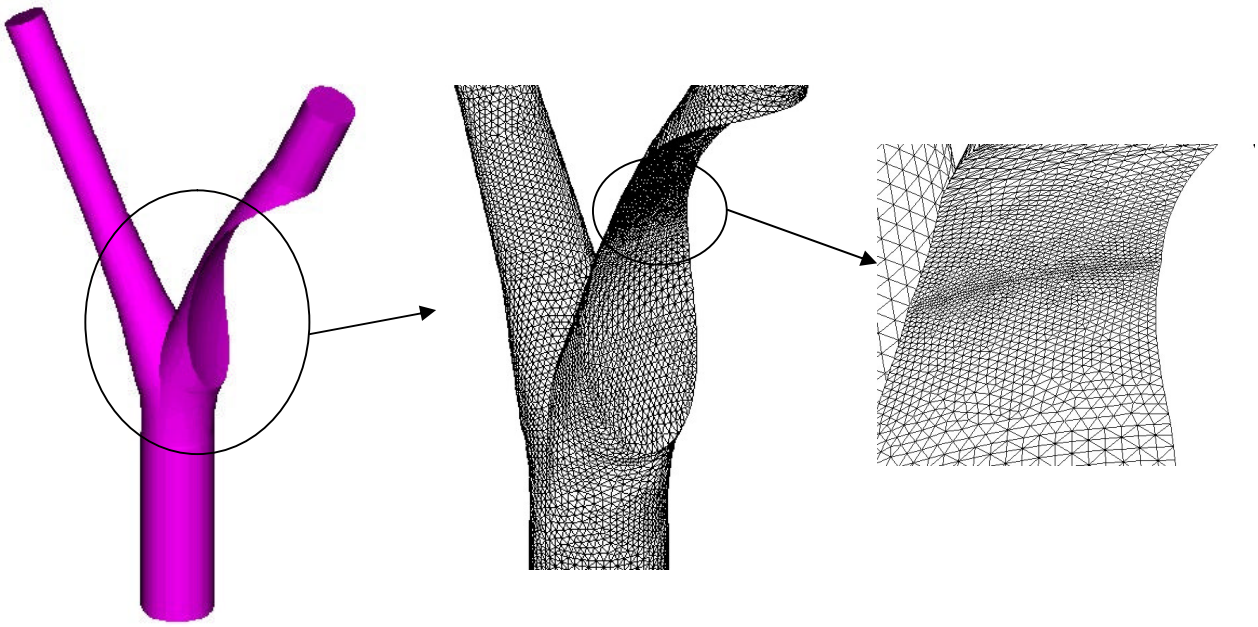

Fig. 6. Case *S95*. Geometry and surface mesh.

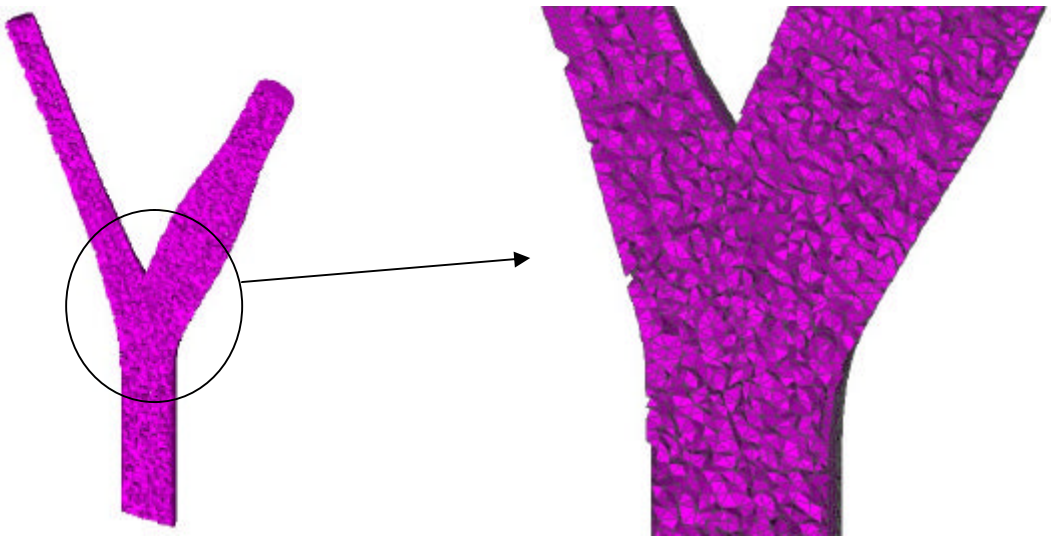

Fig. 7. Case *N*. Volume mesh.

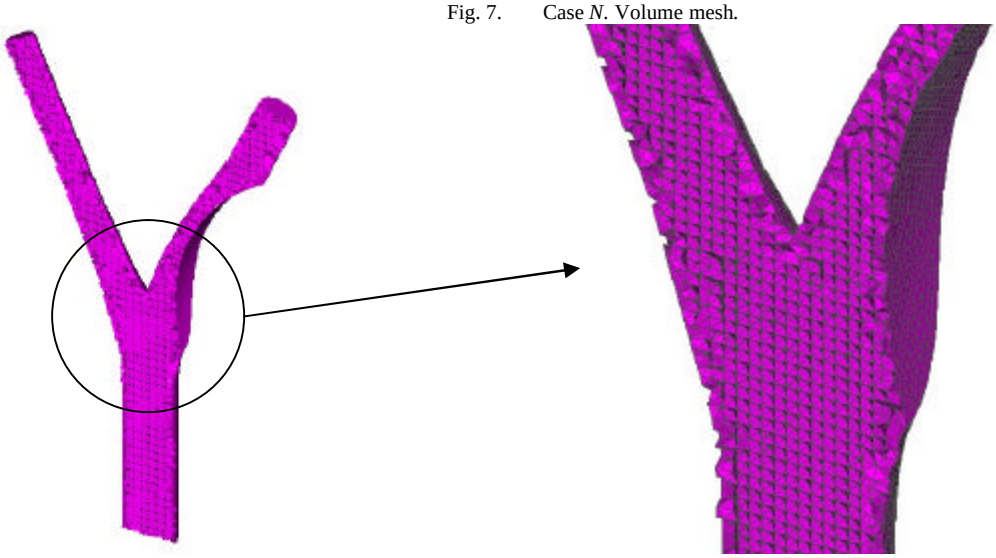

Fig. 8. Case *S80*. Volume mesh.

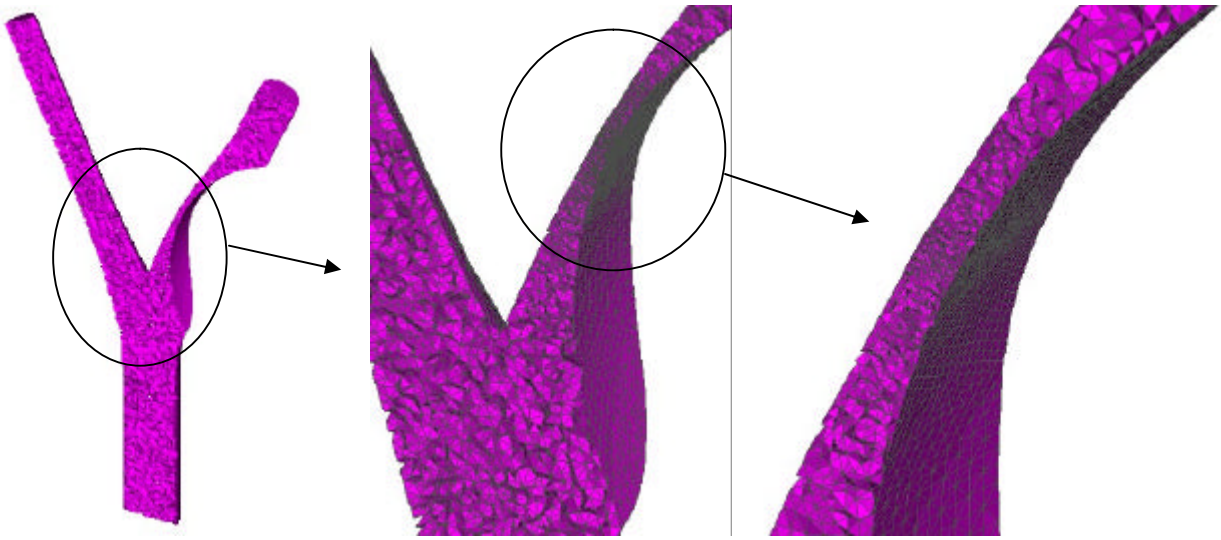

Fig. 9. Case *S95*. Volume mesh.

4 Results

Several results were presented so as to give an idea of the most influent factors regarding the wave morphology inside the human arterial system and the sensibility of such waves with respect to boundary condition at the entrance, the effect of viscoelasticity and the effect of stenosis level. All the cases where solved using the multidimensional model (1D-3D) with an integration time-step of *1.25E-03 sec*. In the present work the viscoelastic parameter *k* is adopted equal to a null value for pure elastic wall behaviour or corresponds to a value of $f = 5^o$ as previously defined. As shown in Fig. 2 the heart period used is of $T = 0.8$ *sec*.

4.1 Influence of heart inflow condition and wall viscoelasticity

In Fig. 10 it is shown a scheme with the points where the results were evaluated, corresponding to the aortic arch -position A -, and to the common carotid -position B-, this one placed at 4 cm from the carotid bifurcation.
First, in Fig. 11 and Fig. 12 the obtained pressure curves on points A and B are presented. It can be noticed a strong dependence of the obtained curves with respect to the different conditions imposed in the entrance. This effect is more evident for the flow rate curves at the common carotid, as shown in Fig. 13.

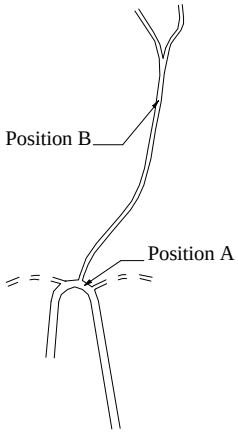

Fig. 10. Chosen positions for the evaluation of results.

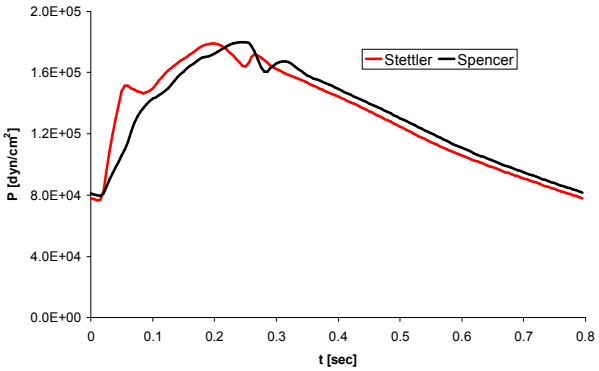

Fig. 11. Pressure curves in A position.

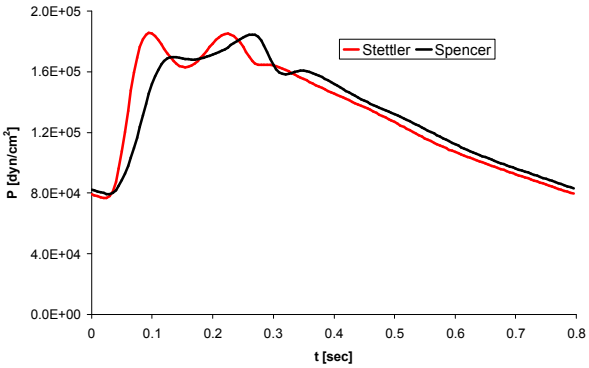

Fig. 12. Pressure curves in B position.

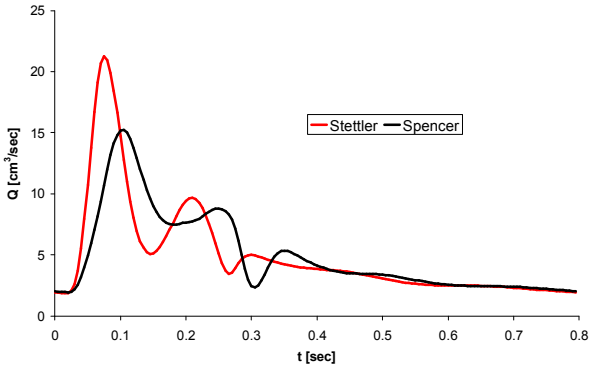

Fig. 13. Flow rate curves in B position.

Next, results at the selected points are compared with respect to experimental data registered by Kelly[20] for the pressure curve in the ascending aorta (see Fig. 14 and Fig. 15) and by Zhao[31] (see Fig. 16 y Fig. 17) for the case of flow and pressure curves in carotid. Both results correspond with the Spencer inflow boundary condition. It can be appreciated that the curves obtained with the proposed multidimensional model acceptably reproduce the main characteristics of those obtained in the above references. It must be taken into account that the plots here shown were obtained with heart frequencies, ejection conditions and parameters of the arterial system parameters that not necessarily match with those reported in the mentioned references. Moreover, such conditions have great variability among subjects, an issue that can be observed from the differences among records from different subjects[31].

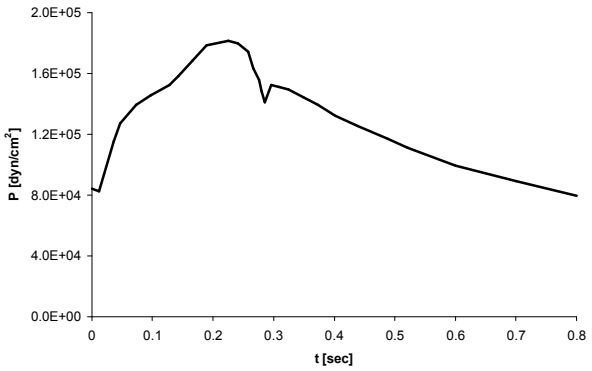

Fig. 14. Experimental measure in the ascending aorta (*Kelly et. al.*).

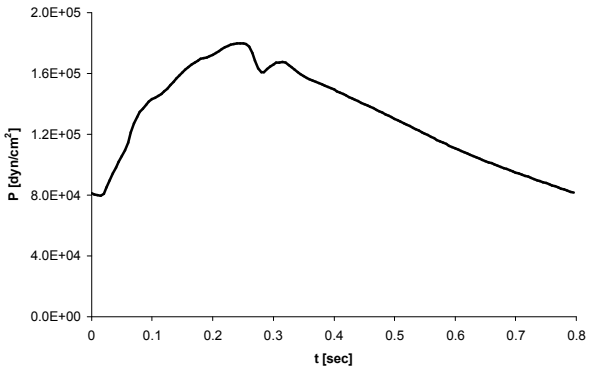

Fig. 15. Results obtained at position A (present work).

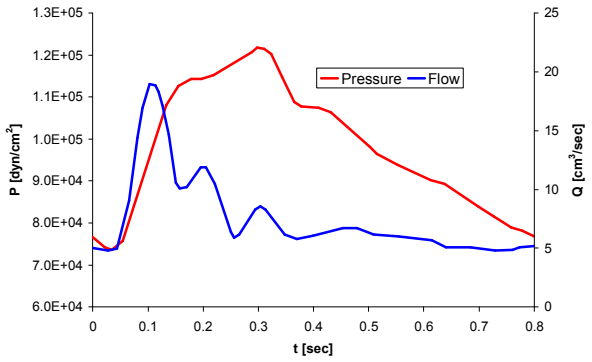

Fig. 16. Experimental records at the common carotid (*Zhao et. al.*).

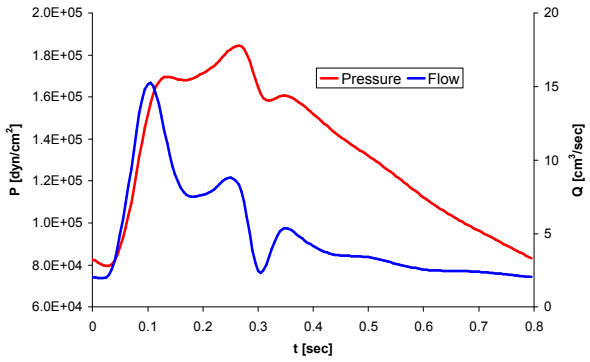

Fig. 17. Results obtained at position B (present work)..

In Fig. 18 it can be clearly observed the increase in the pressure peak along the aorta with increasing distal position (distal augmentation), which is a distinctive characteristic of the arterial system[26].

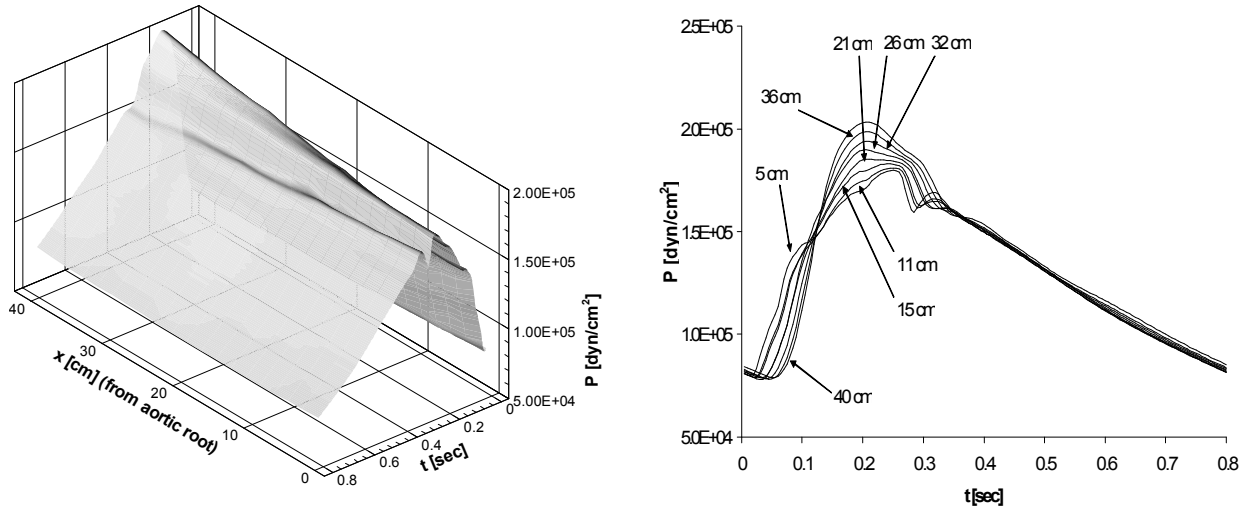

Fig. 18. Variation of the arterial pulse along the aorta (distal augmentation).

Another important aspect addressed is the effect of parietal viscosity. With respect to this issue, the response obtained with a viscoelastic parietal model was compared against a pure elastic one. The results were again evaluated at points A and B using the Spencer curve as inlet condition. Such results are shown in Fig. 19, Fig. 20 and Fig. 21, evidencing that wall viscosity is indispensable to recuperate pulse waveforms that resemble those obtained from *in-vivo* measurements.

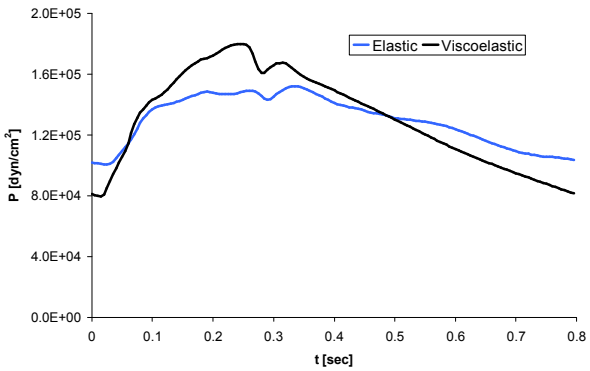

Fig. 19. Pressure curves at point A.

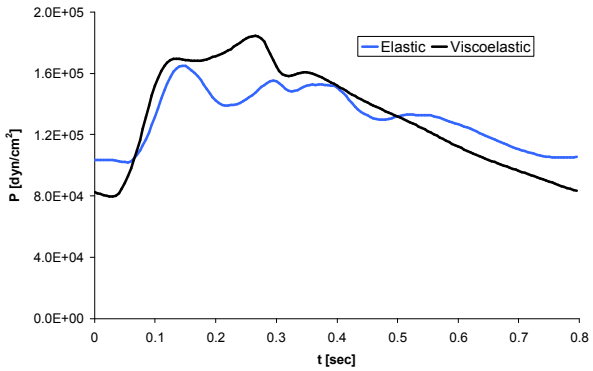

Fig. 20. Pressure curves at point B.

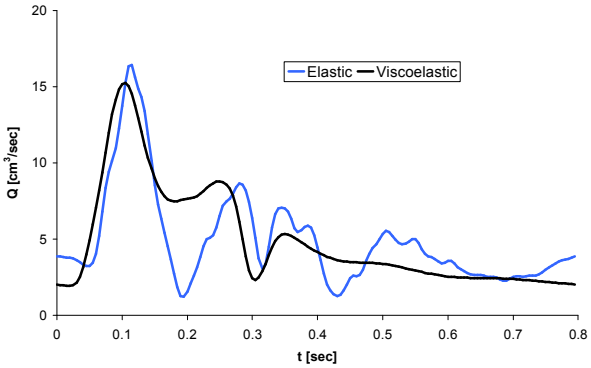

Fig. 21. Flow curves at common carotid (point B).

4.2 Influence of stenosis level

For the proposed stenosis levels (*N*, *S80*, *S95*), curves of pressure and flow were analyzed comparing them on points located at the coupling interfaces. It can be observed that the arterial pulse does not suffer significant perturbations in case *S80* (see Fig. 22, Fig. 23 and Fig. 24). Only in case *S95* appreciable variations for the pressure and blood flow curves are noticeable, especially downstream to the stenosis location (see Fig. 22, Fig. 23 and Fig. 24). The mean flow supplied through the internal carotid shows a 9% reduction with respect to the normal condition. Notice that no vasolidation compensation was assumed.

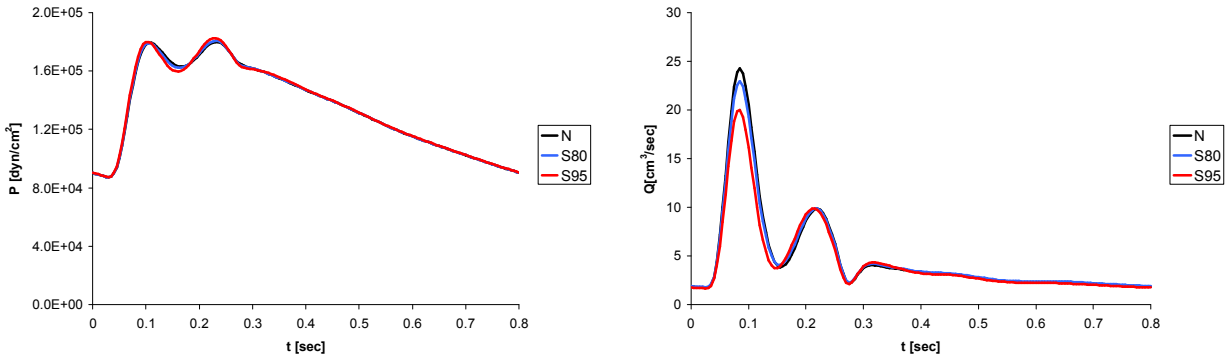

Fig. 22. Comparison of pressure and blood flow curves at the common carotid.

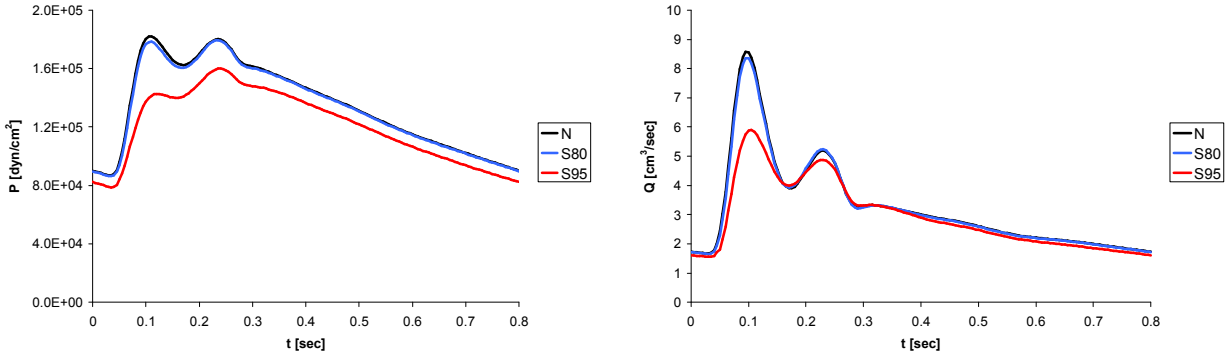

Fig. 23. Comparison of pressure and blood flow curves at the internal carotid.

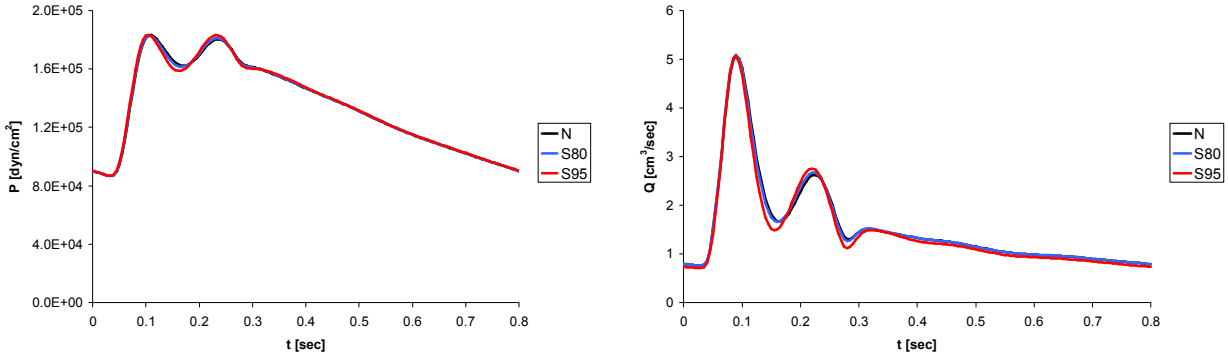

Fig. 24. Comparison of pressure and blood flow curves at the external carotid.

In Fig. 25 pulse waves at the brachial artery are depicted showing that the different stenosis levels have no effect on the results.

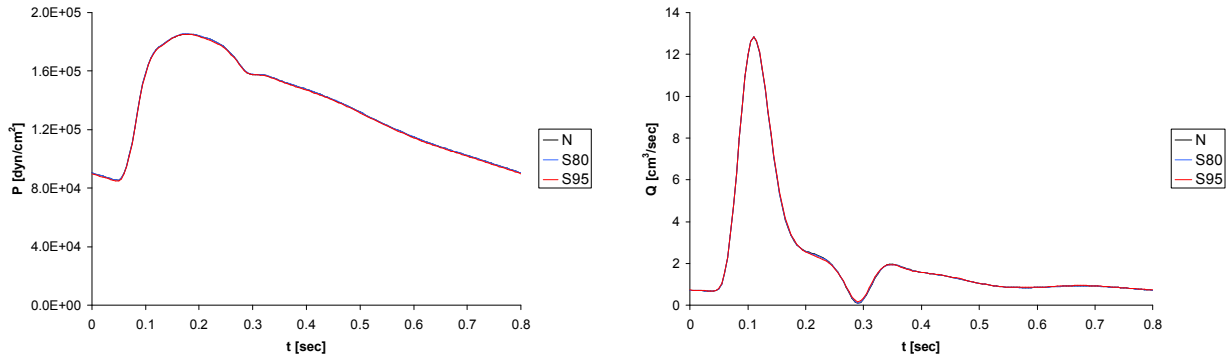

Fig. 25. Comparison of pressure and volume curves at the brachial artery.

The structure of blood flow in the plane of symmetry of the carotid bifurcation 3D model

is presented through Fig. 26 and Fig. 27. In these figures the velocity norm is presented for the two indicated times. We point out that the stenosed region, either in both cases *S80-S95*, corresponds to the zone of quiescent flow in the carotid sinus for the case *N* (see Fig. 27). On the other hand, it can be observed the obvious velocity increment due to the Venturi effect in the stenotic region.

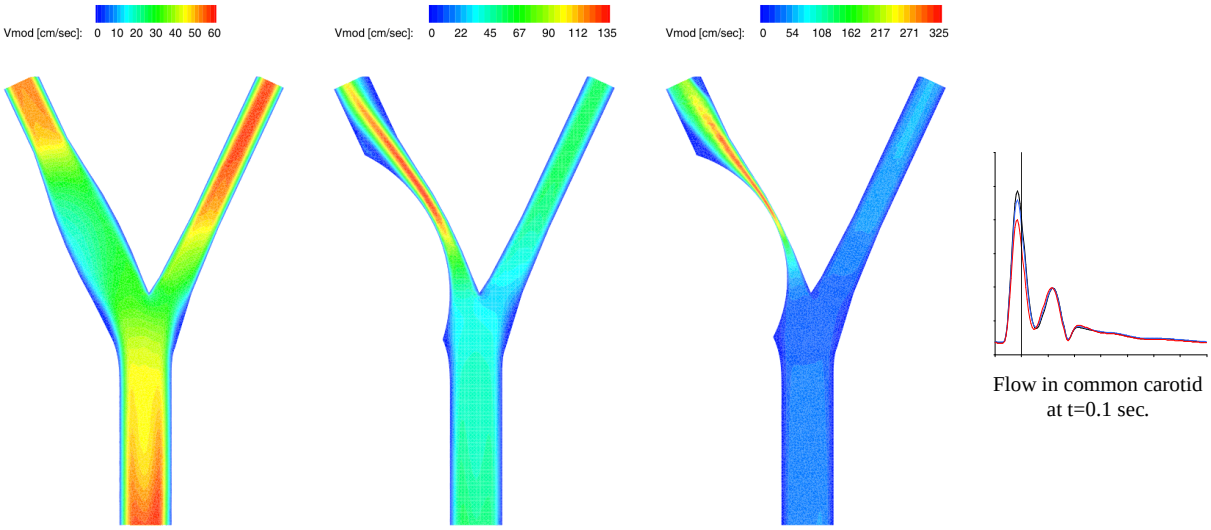

Flow in common carotid
at t=0.1 sec.

Case *N*. Case *S80*. Case *S95*.

Fig. 26. Velocity norm.

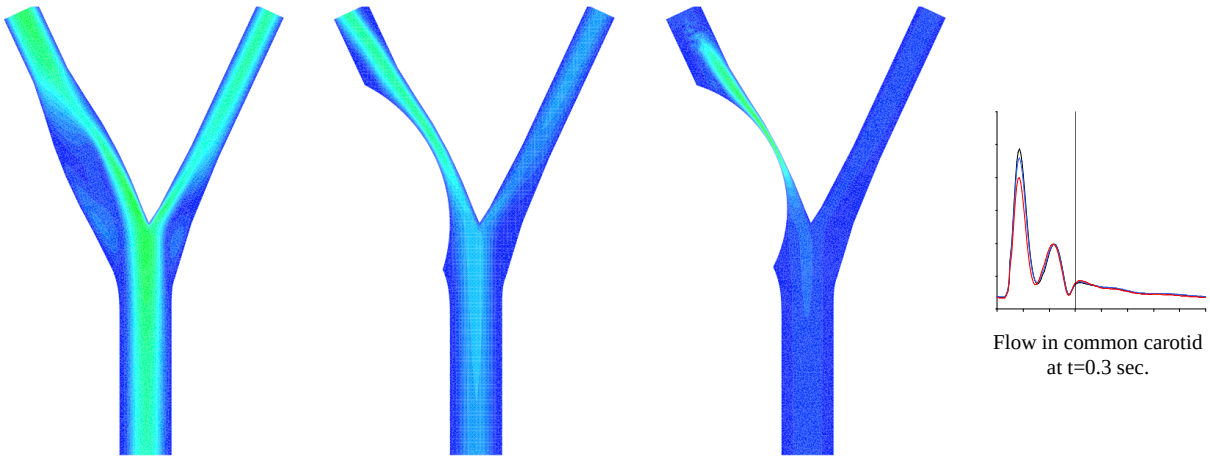

Flow in common carotid
at t=0.3 sec.

Case *N*. Case *S80*. Case *S95*.

Fig. 27. Velocity norm.

In addition, the Oscilatory Shear Index (OSI)[32] for the arterial wall is presented in Fig. 28. We recall the OSI definition,

$$OSI = \frac{1}{2}\left[1 - \frac{\left|\int_0^T t\, dt\right|}{\int_0^T |t|\, dt}\right] \tag{10}$$

where T is the heart period and t is the wall shear stress vector. This index correlates zones where its value approaches to 0.5, with the intima thickening and plaque deposition.

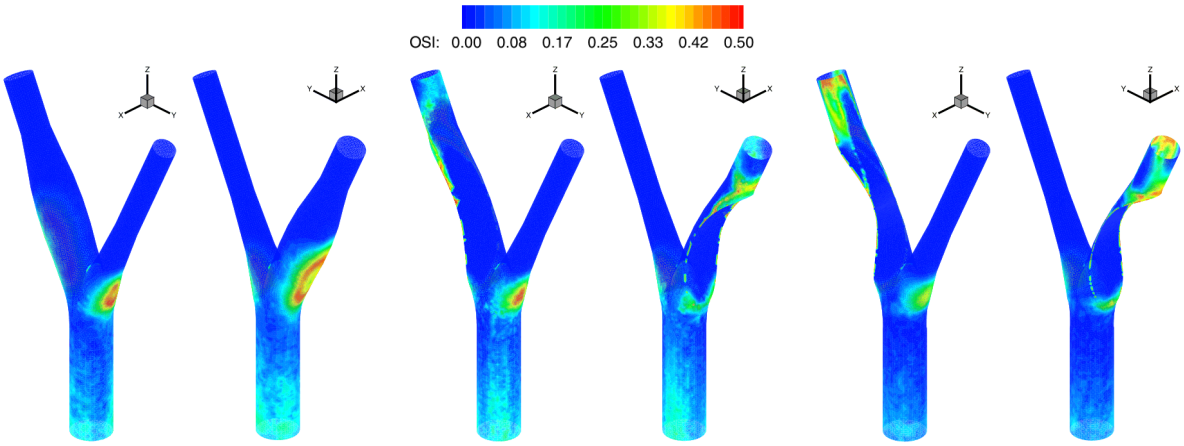

Case *N*. Case *S80*. Case *S95*.

Fig. 28. OSI parameter.

It is observed that the OSI parameter may be a predictive indicator for the localization of stenoses, because it is significantly reduced when the stagnant zone is removed by the presence of the stenosis (see also Fig. 27). Furthermore, considering this behaviour, the OSI could be used for geometry optimization of grafts and anastomosis design.

5 Conclusions

In the present work a coupled 3D-1D model of the complete human arterial system was implemented and some results were contrasted with experimental records reported in the literature. The model is capable of reproducing simultaneously curves of pressure and flow in the carotid artery which resemble the main characteristics of the clinical findings. It has been observed a strong dependence, qualitative and quantitative, of such curves with respect to the heart ejection curve. Also, it has been confirmed the relevance of incorporating parietal viscosity so as to proper conform the arterial pulse. Consequently, the one-dimensional hemodynamic model can be considered as capable of reproducing realistic waveforms. Therefore, it can be used as a valuable tool to provide the appropriate boundary conditions for multidimensional models, better suited for complex descriptions of the structure of the blood flow in specific regions. In fact the 1D model adapt the

coupling boundary conditions automatically, when changes occur on geometry and on other mechanical parameters, either on the two main parts of the model. That is why, it was possible to compare among a healthy carotid and other two cases where different levels of strangling were incorporated in order to evaluate the perturbations they introduced.

In the presented comparison we can appreciate that the perturbations in the arterial pulse become visible only when the stenosis has considerably developed (95%), a fact that is well-known for physicians and physiologists[43]. This leads to a rather disappointing conclusion, as the numerical results confirm the masking of the stenosis in the arterial pulse, which makes very difficult to obtain simple diagnostic indicators from the pulse waveform. On the other hand, the OSI index showed sensibility to the presence of stenoses. This suggest that it could be used for optimal design of grafts and anastomosis, among others surgery procedures, with the aim of reducing the chances of restenosis recurrence.

References

[1] Caro C.G., Fitz-Gerald J.M., Schroter R.C., "Atheroma and arterial wall shear dependent mass transfer mechanism for atherogenesis", Proc. Royal Society of London, Biology, 1971, 177: 109–159.

[2] Hughes T.R.J. "On the threshold of the 21st century", expressions, bulletin for The International Association for Computational Mechanics, Nº8, January 2000.

[3] Giddens D.P., Zarins C.K., Galvov S., "The role of Fluid Mechanics in the Localization and Detection of Atherosclerosis", J. Biomech. Engng, 1993, 115: 588-594.

[4] Anayiotos A.S., Jones S.A., Giddens, Glagov S., Zarins C.K., "Shear Stress at a Compliant Model of the Human Carotid Bifucation", J. Biomech. Engng, 1994, 117: 98-106.

[5] Hyun S., Kleinttreuer C., Archie J.P.Jr., "Hemodynamics analyses of arterial expansions with implications to thrombosis and restenosis", Medical Engineering & Physics, 2000, 22: 13-27.

[6] Vénere M.J., Feijóo R.A., "Generación de Mallas a Partir de Tomografias", MECOM99, Mendoza, Argentina,1999.

[7] Cebral J.R., Yim P.J., Löhner R., Soto O., Choyke P.L., "Blood Flow Modeling in Carotid Arteries with Computational Fluid Dynamics and MR Imaging", Academic Radiology, 2002, 9 (No 11): 1286-1299.

[8] Calamante F., Yim P.J., Cebral J.R., "Estimation of bolus dispersion effects in perfusion MRI using image-based computational fluid dynamics", NeuroImage, 2003, 19: 341–353.

[9] Taylor C.A., Hughes T.J.R., Zarins C.K., "Finite element modeling of blood flow in arteries", Comput. Methods Appl. Mech. Engrg., 1998, 158: 155-196.

[10] Taylor C.A., Engel G., Hughes T.J.R., "Finite element simulation of pulsatile flow through distensible blood vessels", 4th. World Congress on Computational Mechanics, Buenos Aires, 1998.

[11] Avolio A.P, "Multi-branched model of the human arterial system", Med. Biol. Eng. Comp.", 1980, 18: 709-718.
[12] Stergiopulos N., Young D.F., Rogge T.R., "Computer simulation of arterial flow whit applications to arterial and aortic stenoses", J. of Biomechanics, 1992, 25: 1477-1488.
[13] Schaaf, B.W., Abbrecht P.H., "Digital computer simulation of human systemic arterial pulse wave transmission: a nonlinear model", J. Biomechanics Engineering, 1972, 5: 345-364.
[14] Olufsen M.S., "Structured tree outflow condition for blood flow in large systemic arteries", Am. J. Physiol., 1999, 276: 257-268.
[15] Frank Otto, "Die Grundform des arteriellen pulses". Zeitschrift für Biologie, 1899, 37:483-529.
[16] Raines J.K., Jaffrin M.Y., Shapiro A.H., "A computer simulation of arterial dynamics in the human leg", J. of Biomechanics, 1974, 7: 77-91.
[17] Balar S., Rogge T.R., Young D.F., "Computer simulation of blood flow in the human arm", J. of Biomechanics, 1989, 22: 691-697.
[18] Spencer M.P., Deninson A.B., "The square-wave electro-magnetic flowmeter. Theory of operation and design of magnetic probes for clinical and experimental applications", I.R.E. Trans. Med. Elect., 1959, 6: 220-228.
[19] Kelly R., Daley J., Avolio A., O'Rourke M., "Arterial dilation and reduced wave reflection: benefit of dilevalol in hypertension", Hypertension, 1989, 14: 14-21.
[20] Kelly R., Hayward C., Avolio A., O'Rourke M., "Noninvasive determination of age-related changes in the human arterial pulse", Circulation, 1989, 80: 1652-1659
[21] Stettler J.C., Niederer P., Anliker M., "Theoretical analysis of arterial hemodynamics including the influence of bifurcations", Annals of Biomedical Engineering, 1980.
[22] Perktold K., Rappitsch G., "Computer simulation of local blood flow and vessel mechanics in a compliant carotid artery bifurcation model", J. of Biomechanics, 1995, 28: 845-856.
[23] Botnar R. , Rappitsch G., Scheidegger M.B., Liepsch D., Perktold K., Boesiger P. "Hemodynamics in the carotid artery bifurcation: a comparison between numerical simulations and in vitro MRI measurements", J. of Biomech., 2000, 33: 137-144.
[24] Snyder M.F., Rideout V.C., Hillestad R.J., "Computer modeling of the human systemic arterial tree". J. Biomechanics Engineering, 1968, 1: 341-353.
[25] Hyun S., Kleinstreuer C., Archie Jr. J.P., "Computational particle hemodynamics analysis and geometric reconstruction after carotid endarterectomy", Comput. in Biollogy and Medicine, 2001, 31: 365-384.
[26] Nichols W.W., O'Rourke M.F., "McDonald's Blood Flow in Arteries: Theoretical, Experimental and Clinical Principles" Forth Edition, Arnold and Oxford Univ. Press, 1998.
[27] Urquiza S.A., Venere M.J., "An application framework architecture for FEM and other related solvers", pp. 3099-3109, ISSN 1666-6070, MECANICA COMPUTACIONAL Vol.XXI, S. Idelsohn, V. Sonzogni, A. Cardona Eds., CERIDE, Sta Fe, 2002.
[28] Urquiza S.A. ,Reutemann A., Vénere M.J., Feijoo R., "Acoplamiento de modelos unidimensionales y multidimensionales para la resolución de problemas hemodinámicos", ENIEF2001, XII Congress on Numerical Methods and their Applications, October 31 – November 2, 2001, Córdoba – Argentina.

[29] Urquiza S., Blanco P., Lombera G., Venere M. and Feijoo R.. "Coupling Multidimensional Compliant Models For Carotid Artery Blood Flow". Mecánica Computacional Vol. XXII, M. B. Rosales, V. H. Cortínez y D. V. Bambill (Editores) Bahía Blanca, Argentina, Noviembre 2003, pp232-243, AMCA, 2003.

[30] Zhao S.Z., Xu X.Y., Hughes A.D., Thom S.A., Stanton A.V., Ariff B., Long Q., "Blood flow and vessel mechanics in a physiologically realistic model of a human carotid arterial bifurcation", J. of Biomechanics, 2000, 33: 975-984.

[31] Zhao S.Z., Ariff B. , Long Q. , Hughes A.D., Thom S.A. , Stanton A.V., Xu X.Y., "Inter-individual variations in the wall shear stress and mechanical stress distributions at the carotid artery bifurcation of healthy humans", J. of Biomechanics, 2002, 35: 1367-1377.

[32] Ku D.N., Giddens D.P.Zarins C.K., Glagov S., "Pulsatile flow and atherosclerosis in the human carotid bifurcation. Positive correlation between plaque location and low oscillating shear stress", Aterioscl erosis, 1985, 5: 293-302.

[33] Hughes T.J.R., Liu W.K., Zimmermann, "Lagrangian–Eulerian finite element formulation for incompressible viscous flows", Comp. Meth. App. Mech. Engng., 1981, 29: 329–349.

[34] Hughes T.J.R., Brooks A., "A theoretical framework for Petrov-Galerkin methods with discontinuos functions: Application to the stream-upwind procedure", in: Finite Element in Fluids IV, Wiley, London, 1982, 46-65.

[35] Pironneau O., "Finite-element methods for fluids", Wiley, New York, 1989.

[36] Quarteroni A., "Modeling the cardiovascular system: a mathematical challenge", Mathematics Unlimited - 2001 and Beyond, B. Engquist and W. Schmid Eds, 961-972, Springer-Verlag, 2001.

[37] Formaggia L.,Gerbeau J.F., Nobile F., Quarteroni A., "On the coupling of 3D and 1D Navier-Stokes equations for flow problems in compliant vessels, Comp. Meth.App. Mech & Eng., 2001, 191: 561-582.

[38] Formaggia L., Nobile F., Gerbeau J.F., Quarteroni A., "Numerical treatment of defective boundary conditions for the NavierStokes equations", EPFL-DMA Analyse et Analyse Numerique Report n.20, 2000.

[39] Quarteroni A., Tuveri M., Veneziani A., "Computational vascular fluid dynamics: problems, models and methods", Computing and Visualisation in Science, 2000, vol 2, 163-197.

[40] Formaggia L., Nobile F., Quarteroni A., Veneziani A., "Multiscale modelling of the circulatory system: a preliminary analysis", Comput. Visual. Sci., 1999, vol 2 issue 2/3, pag. 75-83.

[41] Bharadvaj B.K., Mabon R.F., Giddens D.P., "Steady flow in a model of the human carotid bifurcation-I. Flow Visualization", J. of Biomechanics, 1982, 15: 349-362.

[42] Bharadvaj B,K., Mabon R.F., Giddens D.P., "Steady flow in a model of the human carotid bifurcation-II. Laser-Doppler anemometer measurements", J. of Biomechanics, 1982, 15: 363-378.

[43] Young D.F. "Fluid Mechanics of Arterial Stenosis", J. of Biomech. Eng., 1979, 101: 157-175.